Materials Horizons

Prediction of Two-Dimensional High-TC f-electron Ferromagnetic Semiconductor

Journal:	*Materials Horizons*
Manuscript ID	MH-COM-02-2020-000183.R1
Article Type:	Communication
Date Submitted by the Author:	14-Mar-2020
Complete List of Authors:	Wang, Bing; Southeast University Zhang, Xiwen; Henan University, Zhang, Yehui; Southeast University Yuan, Shijun; Department of Physics, Southeast University, Guo, Yilv; Southeast University, School of pyhsics Dong, Shuai; Southeast University, Physics Wang, Jinlan; Southeast University, Department of Physics

Two-dimensional (2D) spintronics with the goal of achieving room-temperature Curie temperature (T_C) ferromagnetism with large spin polarization, especially ferromagnetic semiconductors (FMSs), are key to the development and application of spintronic devices. However, the currently demonstrated 2D FMSs suffer from rather low Curie temperatures and the magnetic exchange mechanism is unclear. In this work, reported for the first time, a high Curie temperature 2D FMS in rare-earth halides (GdI_2 monolayer) is achieved with a number of desirable magnetic properties such as near room-temperature T_C, large magnetization, sizable MAE, and charming bipolar magnetic semiconductivity. Most interestingly, a new magnetic coupling mechanism in the 2D regime, namely, *d*-electron-mediated *f-f* coupling mechanism, has been proposed. This intriguing magnetism is originated from the coexistence of effictive *f-f* direct-exchange (Gd_{4f}-Gd_{5d}) and super-exchange (Gd_{5d}-(I_{5p})-Gd_{5d}) interaction. Meanwhile, this monolayer possesses excellent thermal, dynamical and mechanical stabilities and it has great feasibility of experimental exfoliation from its layered bulk. Our work provides a very promising way to realize 2D intrinsic room temperature FMS, and will certainly boost the study of 2D rare-earth magnetism.

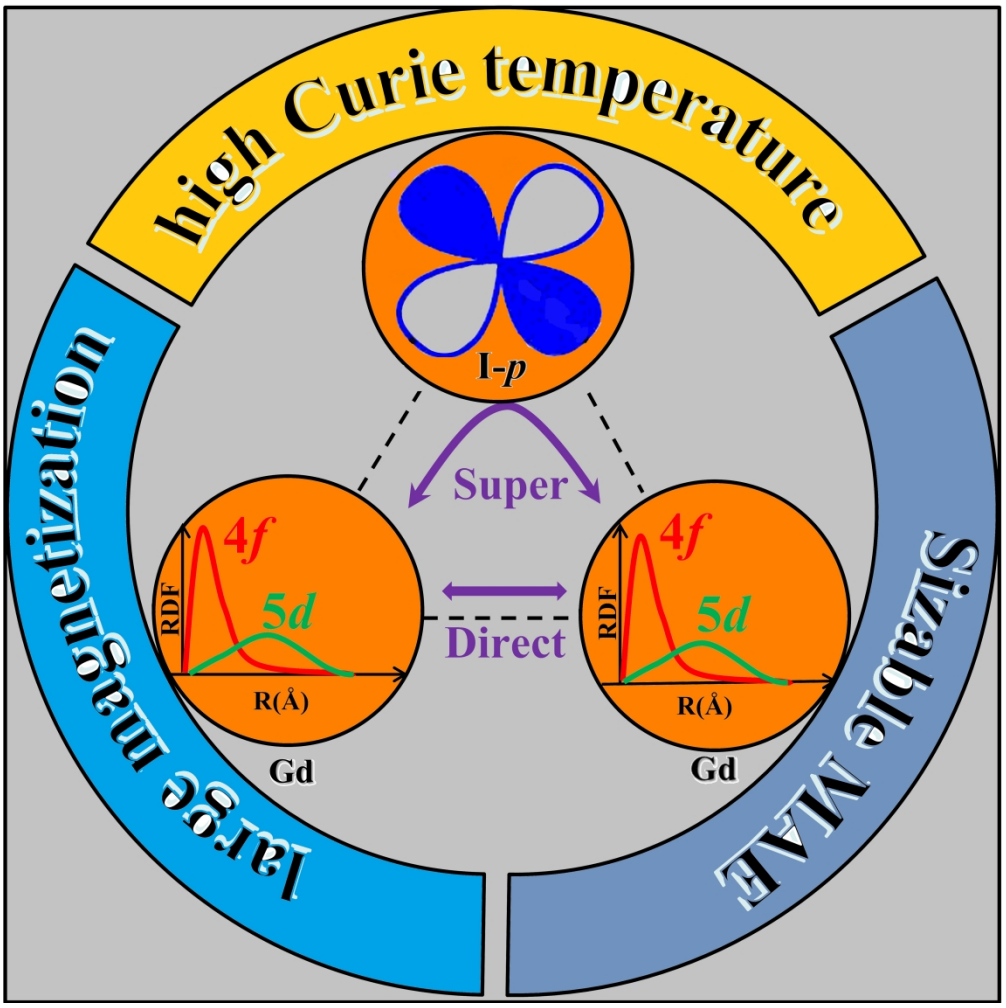

186x185mm (600 x 600 DPI)

Prediction of Two-Dimensional High-T_C *f*-electron Ferromagnetic Semiconductor

Bing Wang,[†,§] Xiwen Zhang,[‡] Yehui Zhang,[†] Shijun Yuan,[†] Yilv Guo,[†] Shuai Dong,*[†] and Jinlan Wang*[†]

[†] School of Physics, Southeast University, Nanjing 211189, China

[§] Institute for Computational Materials Science, School of Physics and Electronics, Henan University, Kaifeng 475004, China

[‡] School of Mechanism Engineering & School of Physics, Southeast University, Nanjing 211189, China

Two-dimensional (2D) ferromagnetic semiconductors (FMSs) exhibit novel spin-dependent electronic and optical properties, opening up exciting opportunities for nanoscale spintronic devices. However, experimentally confirmed 2D FMSs based on transition metal ions are rather limited and their performances are not satisfied, e.g. typically with low Curie temperatures and small magnetic signals. Different from most known 2D magnets based on *d*-electron, here an exotic 2D FMS based on rare-earth ion with *f*-electrons, GdI_2 monolayer, is predicted to own a large magnetization (8 μ_B/f.u.), whose ferromagnetism can survive near room temperature (241 K). In addition, with a small exfoliation energy from its layered van der Waals (vdW) bulk, this GdI_2 monolayer holds excellent dynamical and thermal stabilities, making our prediction promising in experiments. Our prediction not only offers a compelling FMS for spintronics, but also provides an alternative route to acquire more high-performance 2D FMSs, going beyond pure *d*-electron compounds.

Spintronic devices, making use of both charge and spin, have generated world-wide interest due to their faster information operation, lower energy consuming, and higher storage density compared to conventional charge-based electronics.[1-4] One branch of the most promising candidates for spintronics is ferromagnetic semiconductors (FMSs), which have the advantages of combining conventional semiconductor electronics and nonvolatile magnetic storage at finite temperature.[3] FMSs can be used for spin injection, generation, manipulation, and detection, which can be easily implemented in devices by applying nowadays well-developed semiconductor technology.[5] Unfortunately, due to the incompatibility between ferromagnetism and semiconductivity, intrinsic FMSs are rare in nature and their Curie temperatures (T_C) are usually much lower than room temperature, greatly hindering their practical application.[3] Although diluted magnetic semiconductors, which produce ferromagnetism by doping with magnetic elements, were thought to possess potential high-temperature T_C, their reproducible T_C are still limited below 200 K (e.g., 155 K for the most successful Mn-doped GaAs).[6] Besides, problems such as low spin polarization, low dopant solubility, phase separation, bad controllability, and formation of ferromagnetic (FM) clusters appear difficult to be solved.[3, 5] After many years of studies on diluted magnetic semiconductors, the origin of ferromagnetism in these systems remains a subject of debate.[7-9] 'Is it possible to create magnetic semiconductors that work at room temperature?' is still one of the most challenging 125 big questions in science in this century.[10]

The rising of 2D magnetism is expected to play a transformative effect on spintronics applications, such as high integration density and high operation data-processing speed.[11-14] For example, the recent discovery of 2D FMSs, including CrX_3 (X= Cl, Br, I) monolayer [15, 16] and $Cr_2Ge_2Te_6$ bilayer [17], provides a new playground for the applications of 2D spintronics at nanoscale. Besides these synthesized FMSs, other 2D FMSs have also been predicted based on first-principles calculations, such as CrSBr.[18-38] Unfortunately, the T_C of these FMSs are still much below room temperature, although their T_C could be moderately increased by carrier doping,[39-41] strain,[25, 42, 43] and electric-field.[12, 44] Three FMSs were recently predicted to be room-temperature

ones,[20, 45, 46] however their corresponding layered vdW bulk crystals are absent.

Rare-earth elements, which typically own large magnetic moments and high magnetocrystalline anisotropy, are very important in both fundamental scientific researches as well as real applications of high performance magnets,[47-49] However, due to the highly localized characteristic of 4*f* electrons, the direct overlap of 4*f* orbitals between neighbor rare-earth elements, as well as the hybridization between 4*f* orbitals and *p* orbitals of neighbor anions, are mostly negligible. As a result, the direct exchange as well as superexchange mediated by anion are usually very weak between rare-earth magnetic elements, which is the most serious drawback to pursuit high-temperature 4*f* magnetism. Therefore, the 4*f* rare-earth elements seem to be helpless to pursuit high-T_C 2D FMSs, and thus none study of 2D 4*f* magnets has been reported, at least to our best knowledge.

In this work, unexpectedly, we demonstrate a feasibility to realize a promising high-T_C FMS in 2D rare-earth halides (GdI_2 monolayer). The unique exception comes from the coexistence of spin polarized 5*d* orbitals and 4*f* orbitals in Gd^{2+}. The combination of strong Gd_{4f}-Gd_{5d} interaction within each Gd^{2+} ion and strong Gd_{5d}-(I_{5p})-Gd_{5d} interactions leads to a strong ferromagnetism in the 2D limit, i.e. high-T_C (~ 241 K), large magnetization (~ 8 μ_B/f.u.), large magnetic anisotropy energy (~ 553 μeV/Gd). This work not only takes advantage of the properties of rare earth elements with large magnetic moment, but also overcomes the weakness of localized *f* orbitals magnetic exchange in 2D magnetism.

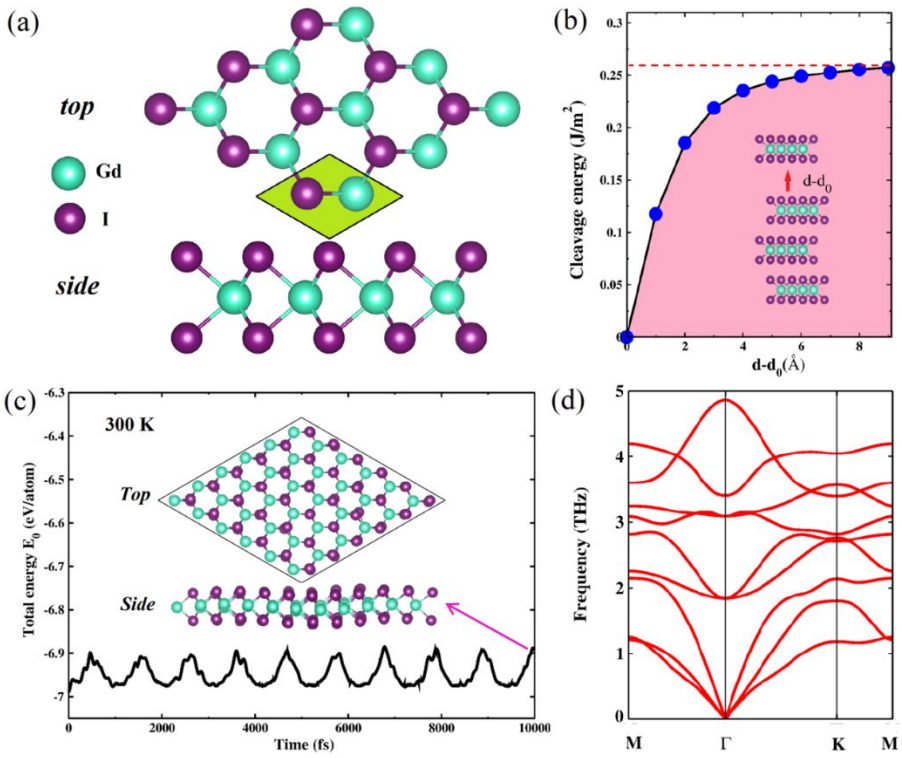

Figure 1. (a) Top and side views of the GdI_2 monolayer. (b) Calculated exfoliation energy vs separation distance (d-d_0), where d_0 indicates the vdW gap between adjacent layers in the bulk crystal. (c) Evolution of total energy from AIMD simulations and the inset is the structure of GdI_2 monolayer at the end of the AIMD simulation after 10 *ps*. (d) Phonon dispersion of the GdI_2 monolayer.

The reason we choose GdI_2 monolayer is as follows. Among all rare-earth elements, Gd is the only room-temperature ferromagnetic rare-earth metal, and some of its compounds also possess high Curie temperatures, such as 352 K for GdScSi.[50] The FM GdI_2 bulk has also been first synthesized by Mee and Corbett [51] with room-temperature T_C (300~340 K).[52-54] In FM GdI_2 bulk, each Gd ion is caged within I_6 trigonal prism (Figure 1a). It has the layered vdW 2*H*-MoS_2-type structure, in which the I-Gd-I sandwich layers are stacked together along the *c*-axis in an AB stacking sequence (Figure S1a). Electron localization function (Figure S1b) confirms that GdI_2 is made up of weak vdW bonded I-Gd-I units, which makes it possible for GdI_2 monolayer to be exfoliated from its layered bulk. Meanwhile, the interlayer FM coupling should be very weak due to the relatively large distance between two interlayer nearest-neighboring Gd atoms (7.84 Å, Figure S1). This weak interlayer interaction also

makes it possible for this monolayer to maintain the room-temperature T_C of the FM bulk crystal.

To explore the possibility of exfoliation of GdI_2 monolayer from its layered bulk crystal, we calculate the cleavage energy from a 4-layer slab. As shown in Figure 1b, the energy increases with the increasing separation distance (d-d_0), and converges to 0.26 J/m^2, which is notably less than the experimental value of graphite (0.36 J/m^2),[55] suggesting the experimental feasibility. Figure 1c shows the corresponding fluctuations of the total potential energies for GdI_2 monolayer during the *ab initio* molecular dynamics (AIMD) simulations and the snapshots of the geometries after annealing at 300 K for 10 ps. The small fluctuations of energy and integrity of original configuration with time evolution confirm its good thermal stability. The absence of imaginary modes in the whole Brillouin zone establishes the dynamic stability of GdI_2 monolayer as well (Figure 1d). Besides, GdI_2 monolayer also meets the mechanical stability Born criteria,[56] and it has good in-plane stiffness (Supporting Information). The small cleavage energy and good stabilities strongly support that 2D GdI_2 monolayer could possibly be prepared in experiment and survive at room temperature.

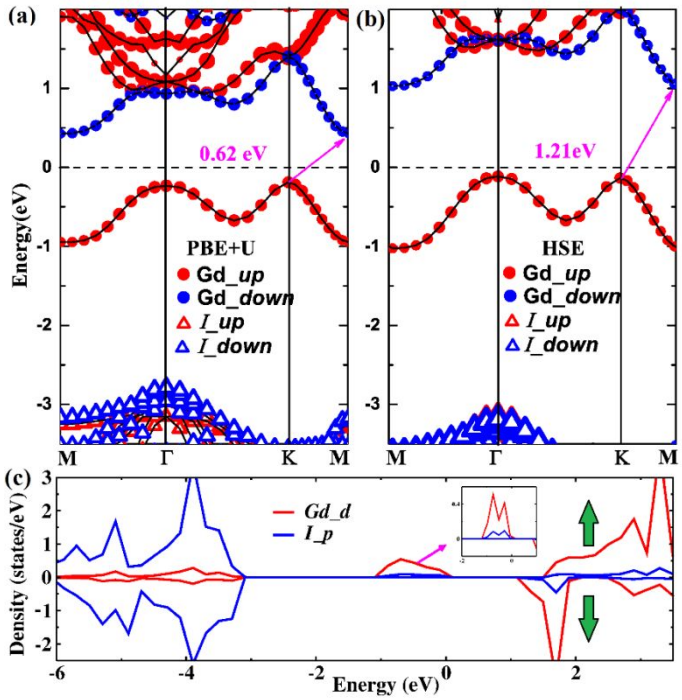

Figure 2. Atom-resolved electronic band structures of GdI_2 monolayer calculated at the PBE+U (a) and HSE06 (b) levels with the corresponding orbital-projected density of

states (c).

The excellent stability and large feasibility of experimental exfoliation of GdI_2 monolayer inspire us to explore its magnetic and electronic properties. The 2×2 supercell of the GdI_2 monolayer with various magnetic orders as schematically shown in Figure S2 is considered to determine the magnetic ground state. Our calculations show that GdI_2 monolayer has a FM ground state with the energy difference between FM and AFM states of 139 meV/Gd. The spin density presented in Figure S2 indicates that the ferromagnetism mainly comes from the contribution of the Gd ion. The spin-polarized DFT calculations using different exchange-correlation functionals show that GdI_2 monolayer is a semiconductor with an indirect band gap of 0.62 eV (PBE+U) and 1.21 eV (HSE06) (Figure 2a and 2b). Note that the HSE06 and PBE+U functionals produce quite similar band structures except for the size of the band gap. Spin-orbit coupling (SOC) effect is also considered and it only decreases the band gap a little bit (Figure S3). Detailed analysis of different atomic components reveals that the conduction and valence bands near the Fermi level are dominated by Gd atom (Figure 2). Very interestingly, GdI_2 monolayer shows a typical bipolar magnetic semiconductor (BMS) feature,[57] in which the valence and conduction bands possess opposite spin-polarization orientation when approaching the Fermi level. Simply by adjusting the position of Fermi level, the unique electronic structure in BMS enables a feasibility to achieve half-metallicity, which can provide 100% spin-polarized current.[58-60] Clearly, the completely spin-polarized currents with reversible spin polarization can be created and controlled by applying a gate voltage, which can be easily applied locally in contrast to magnetic fields.

The calculated spin-polarized atom-projected and orbital-projected density of states (Figure 2c and S4) further reveals that the magnetism in GdI_2 monolayer is mainly contributed by both 4*f* and 5*d* orbitals of Gd atom. All spin-up 4*f* orbitals are occupied while the spin-down ones remain empty (Figure S4). The narrow and high peaks in the DOS plot indicate that the 4*f* electrons of Gd are highly localized. Meanwhile, the 5*d* orbitals are also split into the lower and upper manifolds, which are separated by about 1 eV near the Fermi level. The chemical bonding makes the

completely occupied I 5*p* orbitals mainly centered at ~4 eV below the Fermi level, which are barely affected by the 4*f* states. Figure 2c shows that the top of the valence band is primarily attributed to Gd 5*d* states, hybridized weakly with I 5*p* states.

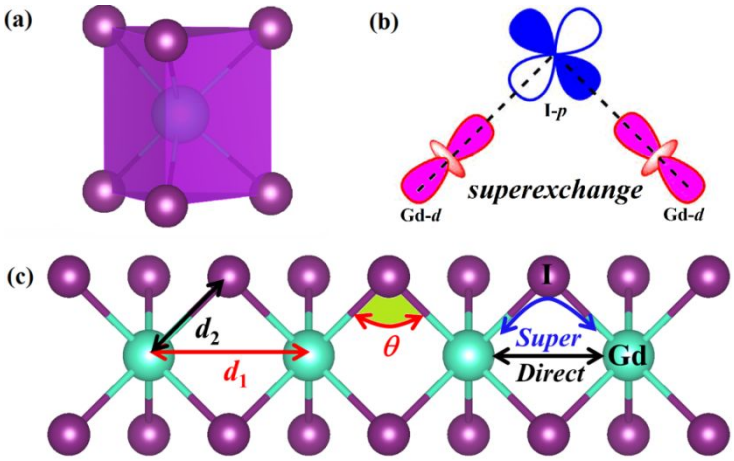

Figure 3. (a) Trigonal prism of six I ions surrounding the Gd ion. (b) & (c) Schematics of Gd-I-Gd superexchange path via *d-p-d* orbitals with the nearest Gd-Gd distance d_1, Gd-I distance d_2, and Gd-I-Gd bond angle θ.

Due to the 4*f* orbitals on Gd atom are highly localized, their direct participation in magnetic exchange coupling should be negligible. In order to understand the nature of FM coupling in GdI_2 monolayer, intr- and inter-atomic interactions need to be considered. For the intratomic interaction, the wave function of 5*d* electrons is more extended than that of 4*f* electrons. Meanwhile, the intratomic Hund interactions between 4*f* and 5*d* electrons is strong. As a result, the 5*d* electrons are spin-polarized in the vicinity of the Fermi level (Figure 2c) and the 4*f* moments will align in a cooperative fashion via the surrounding polarized 5*d* electrons, resulting in the intrinsic large magnetic moments.[61] For the interatomic coupling, the ferromagnetic order can be determined by the coexistence of the direct- and super-exchange interaction. On one hand, the trigonal prismatic crystal field splits 5*d* orbitals into three groups, *a* (d_z^2), e_1 (d_{xy}, d_{x2-y2}), and e_2 (d_{xz}, d_{yz}) (Figure 3a). Then the one 5*d* electron will occupy the spin-up channel on the lowest-energy singlet d_z^2, making GdI_2 monolayer a magnetic semiconductor. In light of Kramers' mechanism, the partially occupied states will lead to the FM direct-exchange interaction (Gd_{5d}-Gd_{5d}) between the nearest neighboring Gd spins. On the other hand, the bond angle of Gd_{5d}-I_{5p}-Gd_{5d}, θ (~82.2°) is close to 90°,

which also prefers the FM coupling according to the Goodenough-Kanamori-Anderson (GKA) rules.[62-64] The schematics of the Gd-I-Gd super-exchange interaction mediated by I anion is plotted in Figure 3b, which arises from the *p*-*d* hybridization between I 5*p* and Gd 5*d* orbitals. As a result, the effective 4*f*-4*f* interaction is FM, mediated by the 5*d*-(5*p*)-5*d* exchanges.

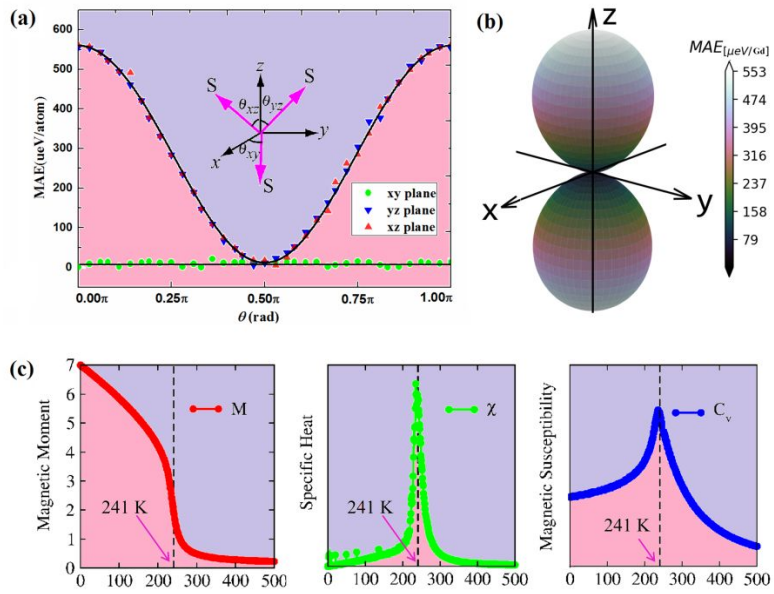

Figure 4. Angular dependence of the magnetic anisotropic energy (MAE) of GdI_2 monolayer with the direction of magnetization lying on three different planes (a) and the whole space (b). The magnetic moment M (red), specific heat C_V (blue), and magnetic susceptibility χ (green) as functions of temperature for GdI_2 monolayer (c).

Magnetic anisotropy is an important requirement for realizing long-range ferromagnetic ordering.[65] Magnetic anisotropy can be scaled by the MAE, which directly correlates with the thermal stability of magnetic data storage. Calculations of total energies including SOC are therefore performed on GdI_2 monolayer to estimate the MAE along the *x* (100), *y* (010), and *z* (001) directions as summarized in Table S1. As a result, this monolayer maybe exhibits an easy magnetic *xy* plane. The angular dependence of the MAE is presented in Figure 4a, which clearly shows that the MAE strongly depends on the direction of magnetization in the *xz* and *yz* plane, whereas the MAE is isotropic in the *xy* plane. As a result, we observe a strong dependence of MAE on the out-of-plane angle of magnetization, similar to that for the VS_2 and $FeCl_2$ monolayer,[66, 67] and in contrast to the easy axis for Fe_3GeTe_2 [68] and CrI_3[15] monolayer.

The strong magnetic anisotropy in this monolayer is further confirmed as shown in Figure 4b which the corresponding MAE through the whole space is displayed. The MAE is zero in plane and reaches a maximum of 553 μeV/Gd perpendicular to the plane, which is comparable to that of CrI_3 monolayer (685 μeV/Cr) and larger than those of $CrXTe_3$ (X = Si, Ge, Sn) monolayers (209, 110, 69 μeV/Cr). [29]

T_C is another key parameter for the practical application of spintronic devices. The Monte Carlo (MC) simulations with Heisenberg model were performed to estimate the T_C of GdI_2 monolayer. The spin Hamiltonian is defined as

$$H = -J\sum_{i,j} S_i \cdot S_j - A(S_i^z)^2$$

where J is the nearest neighboring exchange parameter, S is the spin vector of each atom, and A is anisotropy energy parameter (More details can be found in our previous works[22, 40, 69]). A large 50×50 supercell is used. Using the energy difference between AFM and FM (139 meV/Gd) and normalized S ($|S|$=1), the estimated Heisenberg exchange parameter J is 34.79 meV from $\Delta E = E_{AFM} - E_{FM} = 4J$. After the system reaches equilibrium at a given temperature, the specific heat capacity C_v is calculated by $C_v = \frac{(\langle E^2\rangle - \langle E\rangle^2)}{k_B T^2}$. Providing the exact solution to the spin Hamiltonians, T_C can be estimated from the peak positions of specific heat C_v or magnetic susceptibility χ. The calculated magnetic moment M, C_v, and χ as functions of temperature for GdI_2 monolayer are illustrated in Figure 4c, d, and e, respectively. It can be seen that T_C for GdI_2 monolayer is as high as 241 K, which is significantly higher than those ever reported 2D intrinsic FMSs monolayer from their vdW bulk crystals experimentally or theoretically based on the collected data with our utmost endeavor shown in Figure S5. Meanwhile, using the same approach, our calculated T_C for the recently synthesized $CrCl_3$, $CrBr_3$, and CrI_3 monolayer are around 27 K, 40 K, and 43 K (Figure S6), respectively, which are in excellent agreement with the experimental values of 17 K,[70, 71] 34 K,[16] and 45 K,[15] respectively. Note that the estimated T_C based on Ising models can be as high as 745 K (Figure S7), which is significantly overestimated due to infinite MAE as assumed in the Ising model. The coexistence of near room-temperature ferromagnetic ordering and semiconducting behavior enables GdI_2 monolayer to be a

promising candidate for spintronic applications.

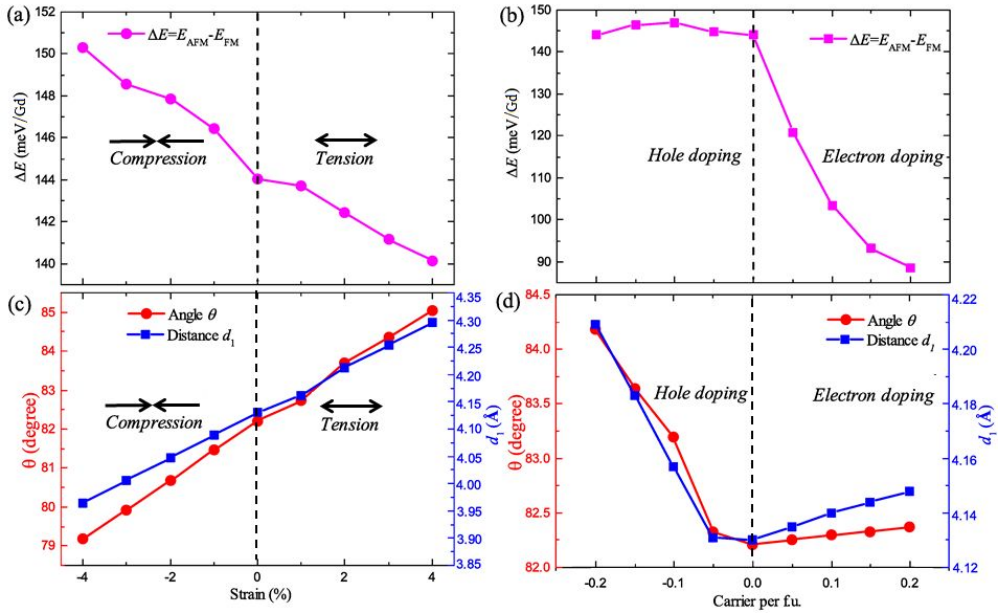

Figure 5. (a) Strain and (b) carrier dependence of the exchange energy $\Delta E = E_{AFM} - E_{FM}$ per unit cell for GdI_2 monolayer. The nearest Gd-Gd distance d_1 and Gd-I-Gd bond angle θ as a function of strain (c) and doping carrier (d).

As we point out above, the synergetic effect of direct- and super-exchange interactions determines the magnetic ground state of GdI_2 monolayer. The distance d_1 and angle θ play an important role on this exchange mechanism. Besides, the intrinsic physical properties would be also affected by the substrate due to the lattice-mismatch-induced strain in the experimental process. Therefore, it is desirable to investigate the effect of the strain and carrier doping on the magnetic behavior. Figure 5a and c show the curves of ΔE, d_1, and θ under the compression and tension strain. ΔE decreases slightly while d_1 and θ increase as the strain is increased. The increased d_1 weakens the direct exchange while the increased angle θ (from 82.2 ^{o} to 85.1^{o}) enhances the super-exchange interaction according to the GKA rule.[72] For the compressive strain, however, the ΔE increases while d_1 and θ decrease as the strain is increased. The decreased d_1 makes the direct exchange becoming more important in determining FM ordering. On the other hand, the bond angle θ of Gd-I-Gd increases monotonically as well and deviates from 90^{o}, thus the super-exchange interaction becomes weak. Importantly, under the range of the strain investigated, the near room-temperature T_C and the BMS characteristic of GdI_2 monolayer are well preserved (Figure S8 and S9), respectively.

The stabilities and possible phase transformation of GdI_2 monolayer under strain was also discussed (Figure S10). For carrier doping, ΔE changes slightly when the hole concentration increases, while gradually decreases when the electron concentration increases (Figure 5b). Meanwhile, the d_1 and angle θ increase with the increasing electron or hole concentration (Figure 5d). With the increasing the carrier doping concentration, GdI_2 monolayer undergoes a BMS to half-metal transition (Figure S11). Meanwhile, under the range of hole doping, near room-temperature T_C of GdI_2 monolayer are also well preserved (Figure S12), while the T_C decreases a little with the increasing electron doping (Figure S13).

In summary, we have demonstrated a promising way to achieve 2D FMS by *d*-electron-mediated *f-f* magnetic coupling mechanism. Owing to the effective *f-f* exchange interactions, a promising 2D intrinsic FMS with near room-temperature T_C (241 K) was predicted as realized in GdI_2 monolayer by using first-principles calculations. The FM states, semiconductivity, and the near room-temperature T_C can be well maintained under the strain conditions. Meanwhile, GdI_2 monolayer possesses BMS property and provides completely spin-polarized currents with reversible spin-polarization simply by applying a gate voltage. Considering the excellent dynamical and thermal stability, and the fact that its cleavage energy is even smaller than that of graphene, the GdI_2 monolayer could be fabricated by mechanical cleavage as graphene. However, we have to point out that the nature of magnetism in monolayer with an easy magnetic *xy* plane still remains an open question, as the 2D *xy* magnetism is not expected to show long-range order at finite temperature. Considering the fact that two-dimensional materials are usually synthesized on the substrate, a suitable substrate (such as heterointerface engineering) might be facilitate the synthesis of GdI_2 monolayer although it is still very challenging in future. Our findings not only provide new insights into the magnetic exchange in rare-earth halides at nanoscale, but also give opportunities for future spintronic investigations and applications.

Method

All the calculations were performed based on the spin-polarized density functional theory (DFT) with the Perdew-Burke-Ernzerhof (PBE) functional in the generalized

gradient approximation (GGA)[73] as implemented in the Vienna *ab initio* simulation package (VASP).[74] The projector-augmented plane wave (PAW) approach was used to represent the ion-electron interaction[75], and the plane-wave cutoff energy was set to 500 eV. Structures were fully relaxed until force and the energy were converged to 0.01 eV $Å^{-1}$ and 10^{-6} eV, respectively. The standard pseudopotential for Gd containing 18 electrons was used, and the $5s^2 5p^6 4f^7 5d^1 6s^2$ valence-electron configuration was considered. The spin−orbit coupling (SOC) has been included in the calculations because of heavy elements. The specific parameters of $U = 9.2$ eV and $J = 1.2$ eV were used for Gd's 4*f* orbitals, which were adopted from previous work[76, 77] and successfully reproduces the experimental magnetic moment of Gd ions in the bulk GdI_2. A detailed test on U_{eff} ($U_{eff} = U - J$) can be found in Figure S14. The HSE06 hybrid functional [78] was also employed to obtain a more accurate band structure and verifies the GGA+U method. We have to point out that, in most cases, the electronic and magnetic properties of 4*f* electron systems is hard to be treated due to the strong correlation and strong spin-orbit coupling of very localized *f* bands.[79] However, Gd^{2+} as studied in our work is an exceptional, whose 4*f* orbitals are half-filled, i.e. $4f^7$. Such half-filled 4*f* bands is simple in physics and can be well-treated in first principles. The comparison between FM and AFM states are added as shown in Figure S15. The spin-orbit coupling was included to get the MAE calculation. Phonon dispersions were calculated by density functional perturbation theory embedded in the phonopy software.[80] AIMD simulations in the NVT ensemble using Nosé–Hoover thermostat lasted for 10 *ps* with a time step of 1.0 *fs*.[81]

ASSOCIATED CONTENT

Supporting Information

The structure and ELF of GdI_2 bulk; Mechanical stability of GdI_2 monolayer; Spin density of FM and AFM states; Band structure with SOC, density of states, and MAE for GdI_2 monolayer; Relationship between band gaps and Curie temperature in monolayer 2D ferromagnetic semiconductors; Magnetic moment as functions of temperature for 2D FM $CrCl_3$, $CrBr_3$, and CrI_3, respectively; Magnetic moment,

magnetic susceptibility, and specific heat as functions of temperature for GdI_2 monolayer based on Ising model; Band structure of GdI_2 monolayer under -4% and 4% strain; Magnetic moment, magnetic susceptibility, and specific heat as functions of temperature for GdI_2 monolayer under -4% and 4% strain; Stability and relative energy of GdI_2 monolayer under different strains; Band structure and Curie temperature of GdI_2 monolayer under different carrier doping concentration; Energy difference of GdI_2 monolayer under different U_{eff} values; Density of states for single Gd atom at FM and AFM states.

AUTHOR INFORMATION

Corresponding Author

*E-mail: jlwang@seu.edu.cn; sdong@seu.edu.cn

Notes

The authors declare no competing financial interest.

ACKNOWLEDGMENTS

This work is supported by the National Key Research and Development Program of China (2017YFA0204800), Natural Science Funds of China (21525311, 11834002, 11674055), the Fundamental Research Funds for the Central Universities (2242019R10021). The authors thank the computational resources from the Big Data Center of Southeast University and National Supercomputing Center in Tianjin.

Reference

1. X. Li and J. Yang, *WIREs Comput. Mol. Sci.*, 2017, **7**, e1314.
2. A. Fert, *Rev. Mod. Phys.*, 2008, **80**, 1517-1530.
3. Y. P. Feng, L. Shen, M. Yang, A. Wang, M. Zeng, Q. Wu, S. Chintalapati and C.-R. Chang, *WIREs Comput. Mol. Sci.*, 2017, **7**, e1313.
4. Y. Zhao, J. J. Zhang, S. Yuan and Z. Chen, *Adv. Functional. Mater.*, 2019, **29**, 1901420.
5. X. Li and J. Yang, *Natl. Sci.Rev.*, 2016, **3**, 365-381.
6. K. Sato, L. Bergqvist, J. Kudrnovský, P. H. Dederichs, O. Eriksson, I. Turek, B. Sanyal, G. Bouzerar, H. Katayama-Yoshida, V. A. Dinh, T. Fukushima, H. Kizaki and R. Zeller, *Rev. Mod. Phys.*, 2010, **82**, 1633-1690.
7. T. Dietl, *Nat. Mater.*, 2010, **9**, 965-974.
8. A. Zunger, S. Lany and H. Raebiger, *Physics*, 2010, **3**, 53.
9. T. Dietl and H. Ohno, *Rev. Mod. Phys.*, 2014, **86**, 187-251.
10. *Science*, 2015, **309**, 78-102.
11. C. G. a. X. Zhang, *Science*, 2019, **363**, eaav4450.

12. H. Li, S. Ruan and Y. J. Zeng, *Adv. Mater.*, 2019, **31**, 1900065.
13. Y. Zhao, J. Gu and Z. Chen, *Adv. Functi. Mater.*, 2019, **29**, 1904782.
14. S. Zhang, R. Xu, W. Duan and X. Zou, *Adv. Funct. Mater.*, 2019, **29**, 1808380.
15. B. Huang, G. Clark, E. Navarro-Moratalla, D. R. Klein, R. Cheng, K. L. Seyler, D. Zhong, E. Schmidgall, M. A. McGuire, D. H. Cobden, W. Yao, D. Xiao, P. Jarillo-Herrero and X. Xu, *Nature*, 2017, **546**, 270-273.
16. Z. Zhang, J. Shang, C. Jiang, A. Rasmita, W. Gao and T. Yu, *Nano Lett.*, 2019, **19**, 3138-3142.
17. C. Gong, L. Li, Z. Li, H. Ji, A. Stern, Y. Xia, T. Cao, W. Bao, C. Wang, Y. Wang, Z. Q. Qiu, R. J. Cava, S. G. Louie, J. Xia and X. Zhang, *Nature*, 2017, **546**, 265-269.
18. N. Miao, B. Xu, L. Zhu, J. Zhou and Z. Sun, *J. Am. Chem. Soc.*, 2018, **140**, 2417-2420.
19. Y. Zhao, L. Lin, Q. Zhou, Y. Li, S. Yuan, Q. Chen, S. Dong and J. Wang, *Nano Lett.*, 2018, **18**, 2943-2949.
20. C. Huang, J. Feng, F. Wu, D. Ahmed, B. Huang, H. Xiang, K. Deng and E. Kan, *J. Am. Chem. Soc.*, 2018, **140**, 11519-11525.
21. Z. Jiang, P. Wang, J. Xing, X. Jiang and J. Zhao, *ACS Appl. Mater. Interfaces*, 2018, **10**, 39032-39039.
22. Y. Guo, Y. Zhang, S. Yuan, B. Wang and J. Wang, *Nanoscale*, 2018, **10**, 18036-18042.
23. S. Zheng, C. Huang, T. Yu, M. Xu, S. Zhang, H. Xu, Y. Liu, E. Kan, Y. Wang and G. Yang, *J. Phys. Chem. Lett.*, 2019, **10**, 2733-2738.
24. H. Yin, C. Liu, G. P. Zheng, Y. Wang and F. Ren, *Appl. Phys. Lett.*, 2019, **114**, 192903.
25. H. Y. Lv, W. J. Lu, X. Luo, X. B. Zhu and Y. P. Sun, *Phys. Rev. B*, 2019, **99**, 134416.
26. C. Wang, X. Zhou, L. Zhou, N.-H. Tong, Z.-Y. Lu and W. Ji, *Sci. Bull.*, 2019, **64**, 293-300.
27. J. He, G. Ding, C. Zhong, S. Li, D. Li and G. Zhang, *J. Mater. Chem. C*, 2019, **7**, 5084-5093.
28. C. Huang, Y. Du, H. Wu, H. Xiang, K. Deng and E. Kan, *Phys. Rev. Lett.*, 2018, **120**, 147601.
29. H. L. Zhuang, Y. Xie, P. R. C. Kent and P. Ganesh, *Phys. Rev. B*, 2015, **92**, 035407.
30. W.-B. Zhang, Q. Qu, P. Zhu and C.-H. Lam, *J. Mater. Chem. C*, 2015, **3**, 12457-12468.
31. X. Li and J. Yang, *J. Mater. Chem. C*, 2014, **2**, 7071.
32. V. V. Kulish and W. Huang, *J. Mater. Chem. C*, 2017, **5**, 8734-8741.
33. Y. Zhu, X. Kong, T. D. Rhone and H. Guo, *Phys. Rev. Mater.*, 2018, **2**, 081001(R).
34. Q. Wu, Y. Zhang, Q. Zhou, J. Wang and X. C. Zeng, *J. Phys. Chem. Lett.*, 2018, **9**, 4260-4266.
35. M. Kan, J. Zhou, Q. Sun, Y. Kawazoe and P. Jena, *J. Phys. Chem. Lett.*, 2013, **4**, 3382-3386.
36. T. Xiao, G. Wang and Y. Liao, *Chem. Phys.*, 2018, **513**, 182-187.
37. Z. Sun, H. Lv, Z. Zhuo, A. Jalil, W. Zhang, X. Wu and J. Yang, *J. Mater. Chem. C*, 2018, **6**, 1248-1254.
38. N. Mounet, M. Gibertini, P. Schwaller, D. Campi, A. Merkys, A. Marrazzo, T. Sohier, I. E. Castelli, A. Cepellotti, G. Pizzi and N. Marzari, *Nat. Nanotechnol.*, 2018, **13**, 246-252.
39. S. Jiang, L. Li, Z. Wang, K. F. Mak and J. Shan, *Nat. Nanotech.*, 2018, **13**, 549-553.
40. B. Wang, Q. Wu, Y. Zhang, Y. Guo, X. Zhang, Q. Zhou, S. Dong and J. Wang, *Nanoscale Horiz.*, 2018, **3**, 551-555.
41. C. Wang, X. Zhou, Y. Pan, J. Qiao, X. Kong, C.-C. Kaun and W. Ji, *Phys. Rev. B*, 2018, **97**, 245409.
42. L. Webster and J. A. Yan, *Phys. Rev. B*, 2018, **98**, 144411.
43. N. Sethulakshmi, A. Mishra, P. M. Ajayan, Y. Kawazoe, A. K. Roy, A. K. Singh and C. S. Tiwary, *Mater. Today*, 2019, **27**, 107-122.

44. Z. Wang, T. Zhang, M. Ding, B. Dong, Y. Li, M. Chen, X. Li, J. Huang, H. Wang, X. Zhao, Y. Li, D. Li, C. Jia, L. Sun, H. Guo, Y. Ye, D. Sun, Y. Chen, T. Yang, J. Zhang, S. Ono, Z. Han and Z. Zhang, *Nat. Nanotechnol.*, 2018, **13**, 554-559.
45. C. Huang, J. Feng, J. Zhou, H. Xiang, K. Deng and E. Kan, *J. Am. Chem. Soc.*, 2019, **141**, 12413-12418.
46. X. Li and J. Yang, *J. Am. Chem. Soc.*, 2019, **141**, 109-112.
47. J. Jensen and A. R. Mackintosh, *Rare earth magnetism*, Clarendon Press Oxford, 1991.
48. B. Tyszka and J. Szade, *J. Alloy. Compd.*, 2003, **354**, 64-71.
49. L. Roy and T. Hughbanks, *J. Solid State Chem.*, 2003, **176**, 294-305.
50. S. Gupta and K. G. Suresh, *J. Alloy. Compd.*, 2015, **618**, 562-606.
51. J. E. Mee and J. D. Corbett, *Inorg. Chem.*, 1965, **4**, 88-93.
52. A. Taraphder, M. S. Laad, L. Craco and A. N. Yaresko, *Phys. Rev. Lett.*, 2008, **101**, 136410.
53. M. Ryazanov, A. Simon and R. K. Kremer, *Phys. Rev. B*, 2008, **77**, 104423.
54. A. Kasten, P. H. Moller and M. Schienle, *Solid State Commun.*, 1984, **51**, 919-921.
55. R. Zacharia, H. Ulbricht and T. Hertel, *Phys. Rev. B*, 2004, **69**, 155406.
56. R. C. Andrew, R. E. Mapasha, A. M. Ukpong and N. Chetty, *Phys. Rev. B*, 2012, **85**, 125428.
57. X. Li, X. Wu, Z. Li, J. Yang and J. G. Hou, *Nanoscale*, 2012, **4**, 5680-5685.
58. H. Cheng, J. Zhou, M. Yang, L. Shen, J. Linghu, Q. Wu, P. Qian and Y. P. Feng, *J. Mater. Chem. C*, 2018, **6**, 8435-8443.
59. Y. Wan, Y. Sun, X. Wu and J. Yang, *J. Phys. Chem. C*, 2018, **122**, 989-994.
60. J. He, G. Ding, C. Zhong, S. Li, D. Li and G. Zhang, *Nanoscale*, 2019, **11** 356-364
61. L. E. Roy, Texas A&M University, 2006.
62. J. B. Goodenough, *Phys. Rev.*, 1955, **100**, 564-573.
63. J. Kanamori, *J. Appl. Phys.*, 1960, **31**, S14-S23.
64. P. W. Anderson, *Phys. Rev.*, 1959, **115**, 2-13.
65. N. D. Mermin and H. Wagner, *Phys. Rev. Lett.*, 1966, **17**, 1133-1136.
66. H. L. Zhuang and R. G. Hennig, *Phys. Rev. B*, 2016, **93**, 054429.
67. M. Ashton, D. Gluhovic, S. B. Sinnott, J. Guo, D. A. Stewart and R. G. Hennig, *Nano Lett.*, 2017, **17**, 5251-5257.
68. H. L. Zhuang, P. R. C. Kent and R. G. Hennig, *Phys. Rev. B*, 2016, **93**, 134407.
69. B. Wang, Y. Zhang, L. Ma, Q. Wu, Y. Guo, X. Zhang and J. Wang, *Nanoscale*, 2019, **11**, 4204-4209.
70. X. Cai, T. Song, N. P. Wilson, G. Clark, M. He, X. Zhang, T. Taniguchi, K. Watanabe, W. Yao, D. Xiao, M. A. McGuire, D. H. Cobden and X. Xu, *Nano Lett*, 2019, **19**, 3993-3998.
71. H. H. Kim, B. Yang, S. Li, S. Jiang, C. Jin, Z. Tao, G. Nichols, F. Sfigakis, S. Zhong and C. Li, *PNAS*, 2019, **116**, 11131-11136.
72. K. Junjiro, *J. Phys. Chem. Solids*, 1959, **10**, 87-98.
73. J. P. Perdew, K. Burke and M. Ernzerhof, *Phys. Rev. Lett.*, 1996, **77**, 3865-3868.
74. G. Kresse and J. Furthmüller, *Phys. Rev. B*, 1996, **54**, 11169-11186.
75. P. E. Blöchl, *Phys. Rev. B*, 1994, **50**, 17953-17979.
76. P. Larson, W. R. L. Lambrecht, A. Chantis and M. van Schilfgaarde, *Phys. Rev. B*, 2007, **75**, 045114.
77. H. Jamnezhad and M. Jafari, *J. Comput. Electron.*, 2017, **16**, 272-279.
78. J. Heyd, G. E. Scuseria and M. Ernzerhof, *J. Chem. Phys.*, 2003, **118**, 8207-8215.

79. M. Casadei, X. Ren, P. Rinke, A. Rubio and M. Scheffler, *Phys Rev Lett*, 2012, **109**, 146402.
80. X. Gonze and C. Lee, *Phys. Rev. B*, 1997, **55**, 10355-10368.
81. G. J. Martyna, M. L. Klein and M. Tuckerman, *J. Chem. Phys.*, 1992, **97**, 2635-2643.